PRAMANA
— journal of
physics

Vol. 74, No. 6
June 2010
pp. 907–917

Chaotic motion of dust particles in planetary magnetospheres

JIA XU, XIN WU* and DA-ZHU MA
Department of Physics, Nanchang University, Nanchang 330031, China
*Corresponding author. E-mail: xwu@ncu.edu.cn

MS received 13 February 2009; revised 1 March 2010; accepted 17 March 2010

Abstract. We numerically investigate the motion of a charged particle in a planetary magnetosphere using several kinds of equatorial plane phase portraits determined by two dynamical parameters: the charge-to-mass ratio and the z-component of the angular momentum. The dependence of chaos on any of the three factors including the two parameters and the energy is mainly discussed. It is found that increasing the energy or the absolute value of the ratio always causes the extent of chaos. However, chaos is weaker for larger angular momentum. Qualitative interpretations to the results obtained are also given.

Keywords. Manifold correction; chaos; planetary magnetospheres.

PACS Nos 02.70.-c; 05.45.-a; 45.20.Jj; 95.10.Fh

1. Introduction

Chaos means that the final dynamical state of a system is exponentially sensitive to extremely small variations of initial conditions. There have been many studies of chaos in celestial mechanics and dynamical astronomy because it can play an important role in determining the dynamical structure and evolution of the solar system [1]. In a series of papers, Wisdom [2–4] used chaos to successfully interpret the origin of the 3:1 Kirkwood gap. Sussman and Wisdom [5] detected the chaotic motion of Pluto when the orbital integration time of each outer planet reaches 845 million years. Besides complicated systems like those, two types of simplified dynamical models that approximate the motion of real objects are usually taken into account. One is the planar, circular, restricted three-body problem that describes a surprising degree of complexity in the structure of the phase space [6]. The other deals with the perturbed Kepler problems [7,8]. Thanks to the existence of perturbations, in most cases the systems change from integrable to near-integrable, even highly non-integrable.

An axisymmetric system consisting of a charged dust particle in a planetary magnetosphere [9–12] is regarded as one of the perturbed Kepler problems. In this model, Newtonian gravitational force of the particle is given by the planet, and perturbed force is mainly from the rotation of the magnetic dipole. Which of the

two forces is dominant? The answer depends on the particle's size. For instance, the gravity force on a 1 μm radius dust particle in Jupiter and Saturn rings is 100 times stronger than the electromagnetic force. On the contrary, the electromagnetic force becomes more important for a small particle of 0.1 μm radius. Perhaps an interesting phenomenon is related to the case of particles in the intermediate range, where the transition of the dominated dynamics between these two distinct dynamical regimes occurs frequently. In this sense, Grotta-Ragazzo *et al* [13] discussed the equatorial dynamics of charged particles. They presented all possible topological equatorial phase portraits, namely, outlines of graphs of the effective potential on the equatorial plane. In fact each portrait is completely dependent on the two dynamical parameters: charge-to-mass ratio and the z-component of the angular momentum. At the same time, a classification of the equilibria on the equatorial plane was given. Then an analysis of the stability of the equilibria and that of separatrices and nearby periodic orbits on the equatorial plane with respect to out-of-equatorial plane perturbations were also provided.

Two points affecting the identification of chaos are worth noting. One is necessary to choose a reliable numerical integrator. A symplectic integrator [14], which can conserve the symplectic structure exactly as the original flow, is very suitable for studying the long-term evolution of Hamiltonian systems. On the other hand, although a traditional numerical scheme (such as a Runge–Kutta algorithm) has an artificial damping or excitation caused by the accumulation of the local truncation error, these artificial factors cannot occur as manifold correction schemes are carried out. Since Nacozy [15] and Baumgarte [16] proposed their ideas of correction approach, manifold corrections have greatly been developed by several authors [17–21]. It should be worth pointing out that a low-order traditional numerical scheme with manifold corrections can be viewed as a fast and higher-precision device to simulate various orbital motions. The other is important to adopt an appropriate method for measuring or finding chaos. Now there have been a number of chaos indicators. It should be pointed out that each of them has its advantages and disadvantages. Lyapunov exponents, as a common indicator of chaos, are independent of the dimension of phase space, but they have some shortcomings [22–25]. The method of Poincaré sections can provide an intuitive, clear portrait for the description of cantori or stochastic layers when the dimension of phase space minus the number of independent first integrals is not more than three. Due to the symmetry of the system with the charged dust particle in the planetary magnetosphere, degrees of freedom about the system are reduced from three to two. In this environment, the method of Poincaré sections should be a good means to describe the dynamics.

Unlike the work of ref. [13], our intention in this paper is to apply a fourth-order Runge–Kutta algorithm in the velocity scaling correction scheme of Ma *et al* [19] to numerically trace the dynamics of orbits out of the equatorial plane by virtue of various possible values of the three parameters such as the charge-to-mass ratio, the angular momentum and the energy. The rest of the paper presents the details. In §2 we introduce the related physical model, and evaluate the accuracy of the numerical method considered. Then, we use Poincaré sections to observe the qualitative evolution of the system for several cases. Interpretations to the results obtained are also given. Finally, §4 summarizes our conclusions.

2. Physical model and integration algorithm

A simplified physical model with a charged dust particle under the influence of Keplerian gravity and a rotating magnetic dipole is given. Its equilibria on the equatorial plane are introduced. Then, a Runge–Kutta family algorithm combined with correction of energy is applied to work out this problem.

2.1 *Physical model*

A charged dust particle in a planetary magnetosphere is mainly subjected to the action of the point-source gravity of the central planet, as the dominant force. Of course, gravitational perturbations and perturbations from non-gravitational forces also affect its motion. The strongest gravitational perturbation, 0.1 to 1% the strength of the point-source gravity, arises from the planet's non-spherical shape, the 'oblateness' represented by the axially symmetric quadrupole (J_2) component in a multipole expansion of gravity. Other gravitational perturbations involve solar gravity, gravity from other planets and attractions of planetary satellites. Electromagnetic (Lorentz) forces and radiation pressure ranging from 0.01 to 1% of the strength of planetary gravity are some of the several non-gravitational forces, and the various drag forces, such as plasma drag, Poynting–Robertson drag, and resonant charge variations, are nearly 10^{-6} times smaller than the gravity. Poynting–Robertson drag is the strongest drag force, while plasma drag is relatively weaker. Although these drag forces are so weak, they can give rise to secular changes in the orbital energy and angular momentum. As to the effect of plasma drag, it is invoked to explain energy dissipation when dust grains are very close to the giant planets. Dust within the synchronous distance loses energy in collision with the plasma and spirals in toward the planet because it moves faster than the plasma, but dust outside the synchronous distance gains energy and drifts away from the planet. This force will eventually damp orbital eccentricities and inclinations (see [26,27] for detailed insight into the action of all the forces).

Note that collisions between dust particles can be neglected under the special circumstance of low dust density. On the other hand, the size of a dust particle in a planetary magnetosphere plays an important role in dominating the dynamics, as mentioned in the Introduction. For smaller submicron-sized grains, the electromagnetic force can greatly exceed the gravity. In this case, the gravitational force becomes too weak to be neglected. For the intermediate range in which both the electromagnetic force and the gravitational force are comparable, and for the case of other negligibly weak perturbations, the system of a charged dust particle in a planetary magnetosphere is simplified as the following classical Hamiltonian formulation

$$H = \frac{1}{2}(p_\rho^2 + p_z^2) + \frac{1}{2\rho^2}\left(p_\phi - \delta\frac{\rho^2}{r^3}\right)^2 + \delta\frac{\rho^2}{r^3} - \frac{1}{r}, \tag{1}$$

where ρ, ϕ and z represent cylindrical coordinates, and $r = \sqrt{\rho^2 + z^2}$. Obviously, p_ϕ, a constant, stands for the z-component of the angular momentum. In addition,

Table 1. A classification of the equilibria on the equatorial plane. Here NoE denotes the number of equilibria and $f_1(\delta) = (6\sqrt{3}|1-\delta|\delta)^{1/3}$.

Case	Conditions	NoE
1	$0 < \delta < 1$, $p_\phi > f_1(\delta)$	3
2	$0 < \delta < 1$, $p_\phi < f_1(\delta)$	1
3	$\delta < 0$, $p_\phi > f_1(\delta)$	1
4	$\delta < 0$, $p_\phi < f_1(\delta)$	3
5	$\delta = 0$, $p_\phi \neq 0$	1
6	$\delta \geq 1$, $p_\phi < f_1(\delta)$	0
7	$\delta \geq 1$, $p_\phi > f_1(\delta)$	2

parameter δ denotes the charge-to-mass ratio in a dimensionless way. For a particle with charge q and mass m, δ is given by

$$\delta = \frac{q}{m}K. \tag{2}$$

Here the constant K depends on the mass M of the planet, the spin angular velocity Ω of the planet, the magnitude $\mathcal{M}$ of the magnetic dipole moment of the planet, the velocity c of light, and the universal constant G of gravitation. It is expressed as $K = \mathcal{M}\Omega/(cMG)$.

The effective potential of the system (1) on the equatorial plane $z = 0$ is of the form

$$U(\rho) = \frac{p_\phi^2}{2\rho^2} - \frac{1}{\rho} + \frac{\delta}{\rho} - \frac{\delta}{\rho^3}p_\phi + \frac{\delta^2}{2\rho^4}. \tag{3}$$

The equilibria on the equatorial plane can be obtained from the equation $U'(\rho) = 0$. Note that a solution of the equation is completely determined by two parameters δ and p_ϕ. Therefore, different possible values of the parameters give different equatorial plane phase portraits. Seven cases about the equilibria are listed in table 1. More details of the physical model and its equilibria on the equatorial plane can be found in refs [9,10,13].

Case 5 indicates that the system (1) is just an integrable Keplerian problem. Its dynamics is very clear to us, and so we do not pay more attention to it. Here we are interested in understanding the structure of phase space of the system (1) for weak electromagnetic forces with $0 < |\delta| < 1$ in each of Cases 1–4.

2.2 *A Runge–Kutta algorithm combined with correction of energy*

Let us take $\delta = 0.1$, $p_\phi = 2$, and energy $E = -0.03147$. Initial conditions are as follows: $\rho = 3.5$, $z = 0$, $p_\rho = 0$, and p_z is a positive square root given by eq. (1). We use a fourth-order Runge–Kutta algorithm (RK4) to solve the system (1) with a fixed step-size of 0.1, and plot the evolution of the energy error with time in figure 1. It is clearly shown that RK4 cannot preserve the energy of this system

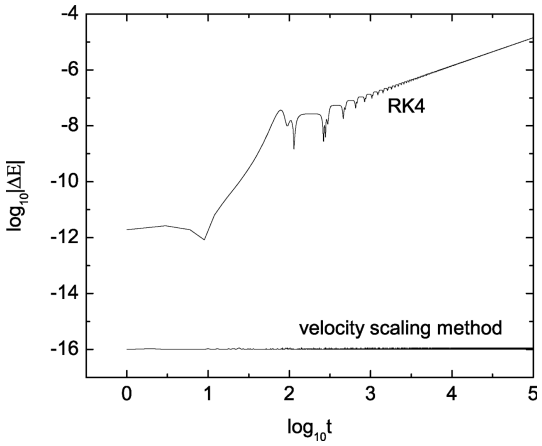

Figure 1. Comparison of energy errors between RK4 and its correction of energy, the velocity scaling method.

(1) although the system is conservative. This is caused by the accumulation of the local truncation error from the numerical scheme.

However, the velocity scaling method of Ma *et al* [19] is a simple tool to get rid of the artificial dissipation of energy. Here are some details of the implementation. Suppose that RK4 gives the system (1) a numerical solution $(p_\rho^*, p_z^*, \rho^*, z^*)$ at time t. Inserting $p_\rho = \lambda p_\rho^*$, $p_z = \lambda p_z^*$, $\rho = \rho^*$ and $z = z^*$ into eq. (1), we have the scale factor of the form

$$\lambda = \sqrt{\frac{2}{p_\rho^{*2} + p_z^{*2}} \left[E - \frac{1}{2\rho^{*2}} \left(p_\phi - \delta \frac{\rho^{*2}}{r^{*3}} \right)^2 - \delta \frac{\rho^{*2}}{r^{*3}} + \frac{1}{r^*} \right]} \tag{4}$$

with $r^* = \sqrt{\rho^{*2} + z^{*2}}$. Obviously the corrected solution (p_ρ, p_z, ρ, z) is more accurate than the numerical solution $(p_\rho^*, p_z^*, \rho^*, z^*)$. For an illustration, ρ and ρ^* (or z and z^*) do not have any difference when the scaling method is used at every integration step, but do after many integration steps. In this way, the energy of the system (1) is rigorously satisfied during the numerical integration. Numerical experiments also support this fact. As expected, figure 1 describes that the energy at every integration step is almost accurate to the order of machine error, 10^{-16}, in a double-precision environment. This ensures the reliability of our numerical approach. Next, a lot of numerical explorations are necessary so as to understand the dynamics of this system.

3. Numerical results and interpretations

In this section, we survey the dynamical transition from order to chaos as one of the three parameters E, δ and p_ϕ is varied, but the others are fixed. Parameter spaces of (δ, p_ϕ) are based on those from the four leading cases in table 1. Then we provide some theoretical analysis to the dependence of chaos on each parameter.

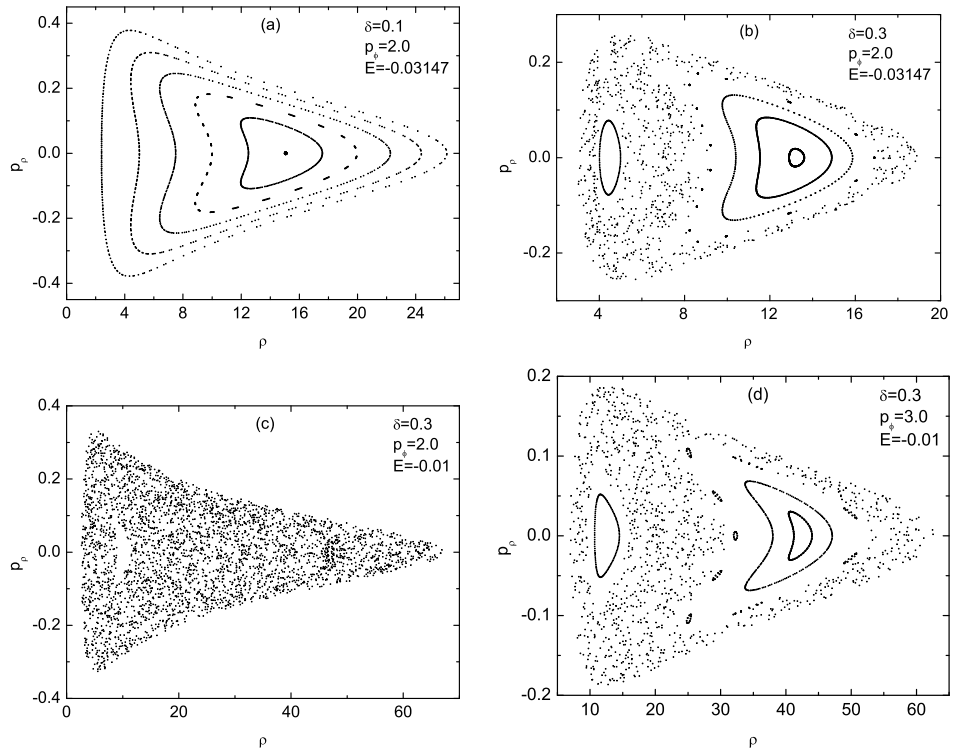

Figure 2. Poincaré sections on the plane $z = 0$ ($p_z < 0$) with $0 < \delta < 1$ and $p_\phi > f_1(\delta)$.

3.1 *Numerical simulations*

Case 1. $0 < \delta < 1$, $p_\phi > f_1(\delta)$

Suppose p_ϕ has a fixed value, 2, and E is -0.03147 or -0.01. In addition, δ is taken as 0.1, 0.2 and 0.3 in sequence. Poincaré sections in figures 2a and 2b display typical effects of varying parameter δ on the dynamics for the given energy, -0.03147. Here are some rich details. In the case of a smaller parameter, $\delta = 0.1$, the electromagnetic force, as a perturbed force, is so weak that the Keplerian gravity completely dominates the dynamics. All KAM tori remain still, but they are twisted, as shown in figure 2a. With the increase of perturbations, some multi-island orbits appear in the case of $\delta = 0.2$, and some tori are destroyed and tend to chaos. As the perturbation becomes stronger, such as $\delta = 0.3$ in figure 2b, a lot of tori given by the original Keplerian gravity die out. Instead, a larger chaotic sea occur. These facts tell us that increasing the charge-to-mass ratio leads to increase in chaos.

As the energy increases, what about the dynamics? Like figure 2b, figure 2c confirms that the chaos will be almost global for $\delta = 0.3$ for the case of $E = -0.01$. Saying this in another way, the larger the energy becomes, the stronger the chaos will be.

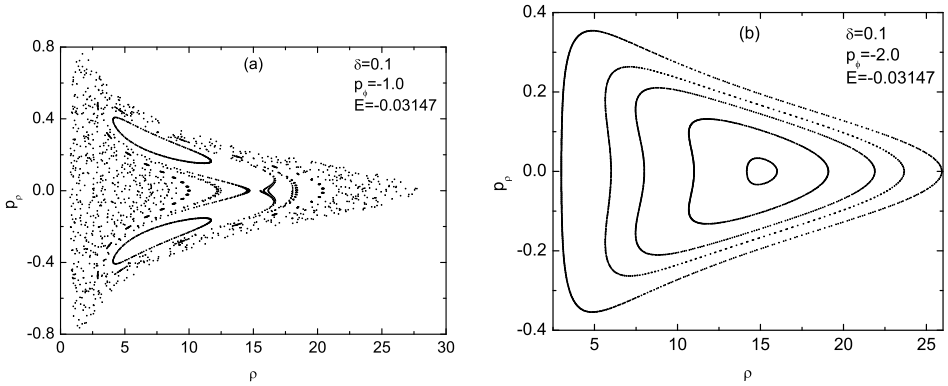

Figure 3. Poincaré sections on the plane $z = 0$ ($p_z < 0$) with $0 < \delta < 1$ and $p_\phi < f_1(\delta)$.

On the other hand, let us demonstrate the dynamics as the angular momentum increases. By comparing figures 2c and 2d, we find that a larger angular momentum corresponds to weaker chaos.

As a result, increasing either the ratio or the energy gives rise to the strength of chaos, but increasing the angular momentum decreases the strength of chaos. Is it true for other cases?

Case 2. $0 < \delta < 1$, $p_\phi < f_1(\delta)$

It is the same as the operation of Case 1 but $p_\phi = -1$ is fixed at first. The relations (not plotted for the sake of saving the space) for the dependence of chaos on parameters δ and E are still similar to those of Case 1. Figures 3a and 2a show that a negative angular momentum causes more chaos than a positive angular momentum. However, chaos is not stronger when the negative angular momentum gets smaller, for example, $p_\phi = -2$ in figure 3b.

Case 3. $\delta < 0$, $p_\phi > f_1(\delta)$

In the light of figures 2c and 4a, one can observe that it is more difficult to yield chaos when δ is negative. If chaos is possible to occur for some negative values of δ, chaos becomes stronger as the negative ratio, δ, is smaller (see figures 4b and 4c for more information). Still it can be concluded from figures 4a and 4b that a larger energy corresponds to stronger chaos. However, figures 4b and 4d illustrate that the transition from chaos to order occurs when the positive angular momentum increases.

Case 4. $\delta < 0$, $p_\phi < f_1(\delta)$

The parameters chosen are the same as those in Case 3 but $p_\phi = -2$. Consequently, the onset of chaos seems to disappear in figure 5.

As stated in the above four cases, some impacts of the three parameters on the dynamics of the system (1) have been described. Increasing energy always increases the extent of chaos. Similarly, chaos is stronger as the absolute value of the charge-to-mass ratio increases. On the contrary, chaos is weaker as the absolute value of the angular momentum increases. Interpretations are offered in the following.

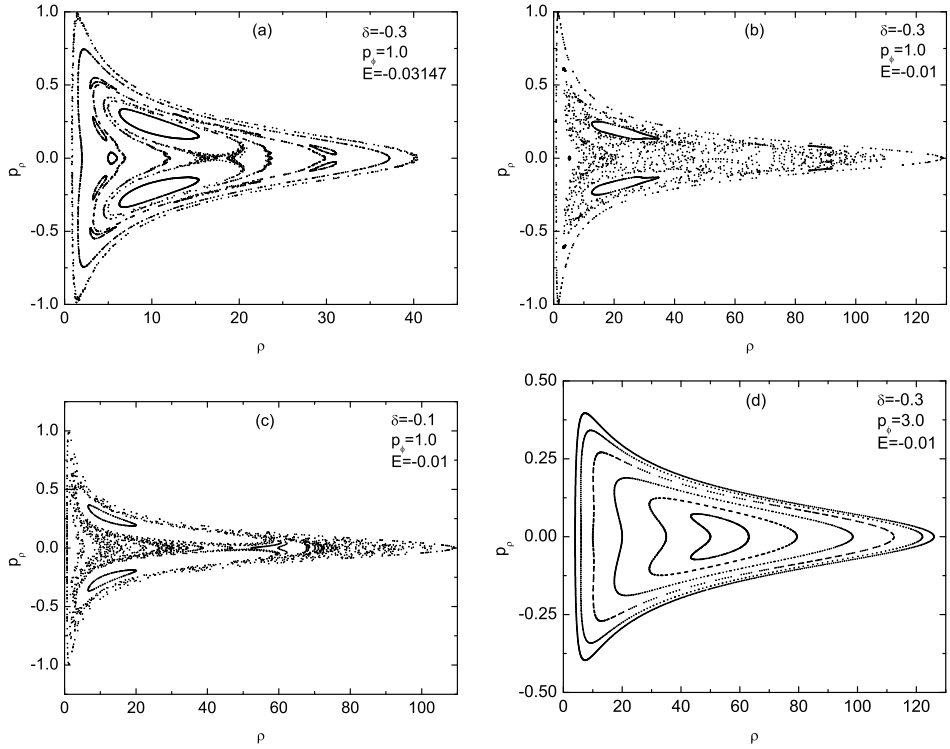

Figure 4. Poincaré sections on the plane $z = 0$ ($p_z < 0$) with $\delta < 0$ and $p_\phi > f_1(\delta)$.

3.2 *Qualitative interpretations*

Our analysis is based on the effective potential

$$U(\rho, z) = \frac{p_\phi^2}{2\rho^2} - \frac{1}{r} + \delta\frac{\rho^2}{r^3} - \delta\frac{p_\phi}{r^3} + \frac{\delta^2}{2}\frac{\rho^2}{r^6} \tag{5}$$

as well as the relation between the magnitude L of the angular momentum, the orbital semimajor axis a and the orbital eccentricity e in the form

$$L = \sqrt{a(1-e^2)}. \tag{6}$$

The first term in the right-hand side of eq. (5) gives a centrifugal inertial force caused by a rotating reference frame, and the second term stands for the Newtonian gravitational potential, while the third and fifth terms correspond to the action of the electromagnetic forces. A point to illustrate is that, for Case 5 without the electromagnetic force in table 1, the equilibrium on the equatorial plane, as a fixed point in this rotating reference frame, implies a circular orbit in an inertial reference frame. In fact, the equilibrium implies that the Keplerian gravity matches with the centrifugal inertial force. It is clearly seen from eq. (5) that the dynamics must

be non-chaotic if the electromagnetic force is extremely weaker than the gravity force. On the contrary, there should be no chaos if the gravitational force becomes negligible compared to the electromagnetic force. A necessary condition for causing chaos is a positive sum of the third to fifth terms in eq. (5). That is to say, a sum of the electromagnetic forces must be a repulsive force.

For the case of $0 < |\delta| < 1$ with $\rho > 1$, usually z is small, so that we have $\rho \sim r$. Thus, the electromagnetic forces are mainly determined by both the third term and the fourth term in eq. (5). Note that the former is more important when p_ϕ is not large enough. Either for $p_\phi > 0$ or for $p_\phi < 0$, the electromagnetic forces always become stronger and stronger as the positive parameter δ is changed from small to large. This increases the extent of chaos. This is what we have seen in figures 2 or 3. On the other hand, for a fixed positive value of δ, chaos should get weaker as the positive parameter p_ϕ increases because the fourth term seems to have an attractive effect. In addition, chaos seems to become more dramatic when $|p_\phi|$ with $p_\phi < 0$ increases because the fourth term turns out to be due to the repulsive action such that the perturbations from the electromagnetic forces get stronger. However, figure 3 does not approve of the result. Here it should be noted that the first term in eq. (5) is more important than the fourth term. In other words, a larger value of L in eq. (6) corresponds to a smaller eccentricity e for a fixed semimajor axis a. This does not result in a closer encounter of the planet with the particle at the pericentre so that both the Keplerian gravity and the electromagnetic force become weaker. In particular, the variation of the latter is more typical. Without doubt, it is more difficult to produce chaos when $\delta < 0$ than when $\delta > 0$ since the third term provides the attractive effect such that the perturbations decrease. This is proved by comparing figures 2 and 4. Of course, the onset of chaos is possible when $p_\phi > 0$ because the fourth and the fifth terms represent the repulsive forces. As δ gets smaller, the repulsive forces get larger. In this sense, the extent of chaos in figures 4b and 4c increases slightly with $|\delta|$ decreasing. Similarly, the growth of p_ϕ (>0) should have raised the extent of chaos for the same negative values of δ and E. But figures 4b and 4d give a different answer as the positive parameter p_ϕ increases. The reason is the same as that of figure 3. If $p_\phi < 0$, there is no great chance for the appearance of chaos because the fourth term seems attractive. What has happened in figure 5 is not unexpected. As far as the dependence of chaos on the energy is concerned, it can be seen easily from eq. (6) that the chaos increases with the energy. For a given L, a larger energy leads to a larger semimajor axis. Meanwhile, the eccentricity becomes larger. Thus the perturbation is stronger at the pericentre.

In order to clearly express the results above, we list table 2 in which effects of the dynamical parameters on chaos are given. In short, our numerical results are fully coincided with these analysis.

4. Summary

We study the motion of charged dust particles under the action of Newtonian gravitational and weak electromagnetic forces. The dynamics depends on three dynamical parameters, the charge-to-mass ratio δ, the z-component p_ϕ of the angular

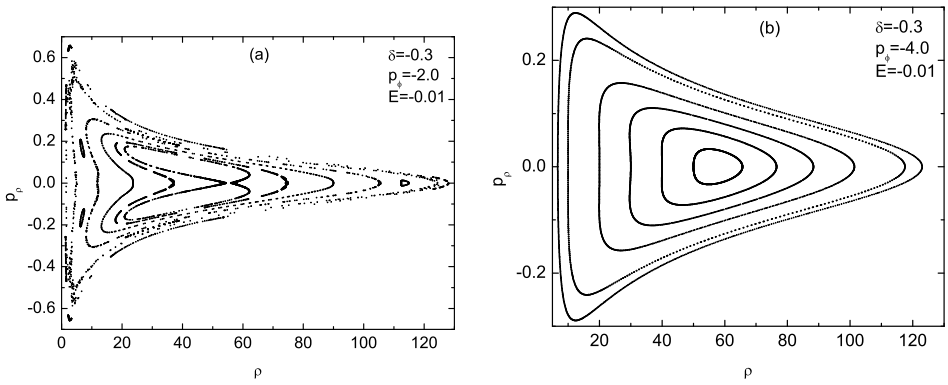

Figure 5. Poincaré sections on the plane $z = 0$ ($p_z < 0$) with $\delta < 0$ and $p_\phi < f_1(\delta)$.

Table 2. Chaos depending on one varying parameter in weak electromagnetic fields with $0 < |\delta| < 1$. In col. (1) two parameters are fixed, while each parameter in cols (2)–(6) is varied from small to large. The symbol $\uparrow$ means increasing, and $\downarrow$ means decreasing. $\Downarrow$ indicates that it is rather difficult to occur chaos. Even if chaos can exist, the extent of chaos diminishes by increasing a certain parameter. – denotes no comparison between fixed parameters and one varying parameter.

Fixed\Varying	$\uparrow \delta > 0$	$\uparrow \delta < 0$	$\uparrow p_\phi > 0$	$\uparrow p_\phi < 0$	$\uparrow E < 0$
$\delta > 0$, E	–	–	$\downarrow$	$\uparrow$	–
$\delta < 0$, E	–	–	$\downarrow$	$\Uparrow$	–
$p_\phi > 0$, E	$\uparrow$	$\downarrow$	–	–	–
$p_\phi < 0$, E	$\uparrow$	$\Downarrow$	–	–	–
$\delta^2 + p_\phi^2 \neq 0$	–	–	–	–	$\uparrow$

momentum and the energy E. Numerical and analytical methods discuss the transition from order to chaos as one parameter is varied but the other two parameters remain invariant. Under some necessary conditions for the occurrence of chaos, increasing the energy always leads to the strength of chaos. In addition, chaos is stronger as the absolute value of the ratio increases. On the contrary, chaos is weaker as the absolute value of the angular momentum increases. Especially, chaos is very difficult to occur if $\delta < 0$ and $p_\phi < 0$.

Acknowledgements

The authors are very grateful to the referee for useful suggestions. This research is supported by the Natural Science Foundation of China under Contract No. 10873007. It is also supported by Science Foundation of Jiangxi Education Bureau (GJJ09072), and the Program for Innovative Research Team of Nanchang University.

References

[1] G Contopoulos, *Order and chaos in dynamical astronomy* (Springer Verlag, Berlin, 2002)
[2] J Wisdom, *Astron. J.* **87**, 577 (1982)
[3] J Wisdom, *Icarus* **56**, 51 (1983)
[4] J Wisdom, *Icarus* **63**, 272 (1985)
[5] G J Sussman and J Wisdom, *Science* **241**, 433 (1988)
[6] C D Murray and S F Dermott, *Solar system dynamics* (Cambridge University Press, Cambridge, 1999)
[7] W M Vieira and P S Letelier, *Astrophys. J.* **513**, 383 (1999)
[8] B Cordani, *Regular and Chaotic Dynamics* **9(3)**, 351 (2004)
[9] J E Howard, M Horányi and G R Stewart, *Phys. Rev. Lett.* **83**, 3993 (1999)
[10] J E Howard, H R Dullin and M Horányi, *Phys. Rev. Lett.* **84**, 3244 (2000)
[11] H R Dullin, M Horányi and J E Howard, *Physica* **D171**, 178 (2002)
[12] M Iñarrea, V Lanchares, J F Palacian, A I Pascual, J P Salas and P Yanguas, *Physica* **D197**, 242 (2004)
[13] C Grotta-Ragazzo, M Kulesza and P A S Salomão, *Physica* **D225**, 169 (2007)
[14] J Wisdom and M Holman, *Astron. J.* **102**, 1528 (1991)
[15] P E Nacozy, *Ap&SS* **14**, 40 (1971)
[16] J Baumgarte, *Celest. Mech.* **5**, 490 (1972)
[17] T Fukushima, *Astron. J.* **126**, 1097 (2003)
[18] X Wu, T Y Huang, X S Wan and H Zhang, *Astron. J.* **133**, 2643 (2007)
[19] D Z Ma, X Wu and J F Zhu, *New Astronomy* **13**, 216 (2008)
[20] D Z Ma, X Wu and F Y Liu, *Int. J. Mod. Phys.* **C19(9)**, 1411 (2008)
[21] D Z Ma, X Wu and S Y Zhong, *Astrophys. J.* **687**, 1294 (2008)
[22] X Wu and T Y Huang, *Phys. Lett.* **A313**, 77 (2003)
[23] X Wu, T Y Huang and H Zhang, *Phys. Rev.* **D74**, 083001 (2006)
[24] X Wu and Y Xie, *Phys. Rev.* **D76**, 124004 (2007)
[25] X Wu and Y Xie, *Phys. Rev.* **D77**, 103012 (2008)
[26] J A Burns, *Am. J. Phys.* **44**, 944 (1976)
[27] J A Burns, P L Lamy and S Soter, *Icarus* **40**, 1 (1979)